



# Electrodynamics of type-II superconductor with periodic pinning array

R.F. Hung<sup>a,\*</sup>, D. Berco<sup>b</sup>, I.Ya. Shapiro<sup>c</sup>, B. Shapiro<sup>c</sup>, B. Rosenstein<sup>a</sup>

<sup>a</sup> Department of Electrophysics, National Chiao Tung University, Hsinchu, Taiwan, ROC,

<sup>b</sup> Department of Electronic Engineering, National Chiao Tung University, Hsinchu, Taiwan, ROC,

<sup>c</sup> Department of Physics, Institute of Superconductivity, Bar-Ilan University, 52900 Ramat-Gan, Israel

## ARTICLE INFO

### Article history:

Received 26 February 2010

Received in revised form 3 July 2010

Accepted 12 July 2010

Available online 16 July 2010

### Keywords:

Superconductivity

Vortex

Pinning array

## ABSTRACT

Static and dynamic distribution of the superconducting condensate order parameters and current density is studied by numerical simulation of the 2D time-dependent Ginzburg–Landau equations. The vortex flux lattice in layered type-II superconductors under magnetic field above the lower critical field is described by the order parameters. Moreover, the pinning effect has been considered in this work. The Abrikosov lattice which is hexagonal in the static case is deformed due to the size of pinning centers. The dynamical order parameters distribution shows that the vortex transport (flux flow) is conducted via diffusive motion of the so-called interstitial vortices. The trajectories for interstitial vortices with different sizes of pinning centers are shown.

© 2010 Elsevier B.V. All rights reserved.

## 1. Introduction

The great interest in the problem of magnetic flux pinning in type-II superconductors is associated with its relevance to technological applications of superconductivity. An important challenge in applications of type-II superconductors is achieving optimal critical currents under given magnetic fields. This requires preventing depinning of Abrikosov vortices during the formation of the resistive state under the applied current. The critical current can be significantly increased at a matching field when the number of Abrikosov flux lines is equal to the number of pinning centers. When the current exceeds the critical value, the vortices move thus inducing voltage. The dynamic behavior of the Abrikosov flux lattice is strongly influenced by the pinning array. In early experiments the distances between the pinning centers,  $d$ , were larger than magnetic penetration depth. Correspondingly the magnetic fields were mostly close to  $H_{c1}$  [2], so that vortices were well isolated within the applicability range of the London approximation [3]; more recently the trend was in the direction of smaller distances between the pinning centers, approaching the coherence length  $\xi$  and consequently larger fields approaching  $H_{c2}$ . Two strategies were employed. The standard one is reducing  $d$ , and the second is increasing the coherence length by tuning the field towards  $H_{c2}(T)$  [1]. In this region the London approximation is not valid and one has to use the more appropriate time-dependent Ginzburg–Landau (TDGL) approach. In the present note we address this problem.

## 2. Model

The order parameter characterizing the superconducting state is calculated numerically for a periodic array of pins (i.e. “nanosolid”). The configurations of the vortex lattice under different pinning arrays (triangle, square) and different pinning center sizes are studied. In addition the trajectory of interstitial vortices are calculated. The relaxation dynamics of Abrikosov vortices in a superconductor with an electric field is described by TDGL equation

$$\frac{\partial}{\partial \tau} \psi = - \frac{\partial}{\partial \psi^*} f_{GL}, \quad (1)$$

where the dimensionless free energy is

$$f_{GL} = \int d\mathbf{r} |\mathbf{D}\psi|^* + \left[ -\frac{1-t}{2} + W(r) \right] \psi^* \psi + \frac{1}{2} (\psi^* \psi)^2. \quad (2)$$

The dimensionless parameter is  $\psi = \frac{1}{\sqrt{2}\psi_0} \Psi$ ,  $\Psi_0 = \sqrt{\alpha T_c / \beta}$  with standard notations for the GL coefficients, see [4,5]. The unit of length is  $\xi$ , while the unit of time characterizing the relaxation is  $t_{GL} = \gamma \xi^2 / 2$ , where  $\gamma$  is an inverse diffusion constant,  $t \equiv T / T_c$  denotes the dimensionless magnetic and electric fields are  $h = B / H_{c2}$  and  $\epsilon = E / E_{GL}$ , where  $E_{GL} = ct_{GL} H_{c2} / \xi$ . Pinning is described by  $W(\mathbf{r}) = \sum_a w(\mathbf{r} - \mathbf{r}_a)$ . We assume that  $\kappa = \lambda / \xi \gg 1$ . This means that the magnetization is smaller than the field by a factor  $1/\kappa^2$  and consequently (for magnetic field few times larger than  $H_{c1}$ )  $B \approx H$ . The magnetic field  $\mathbf{B} = \nabla \times \mathbf{A}$  therefore is homogeneous and constant, where  $\mathbf{A}$  is the vector potential. The current density  $\mathbf{j} = \mathbf{j}_n + \mathbf{j}_s$  has the normal and the supercurrent components

$$\mathbf{j}_n = \epsilon, \quad \mathbf{j}_s = \frac{i}{2} (\psi^* \mathbf{D}\psi - \psi \mathbf{D}\psi^*), \quad (3)$$

\* Corresponding author.

E-mail address: vortexbar@yahoo.com (R.F. Hung).

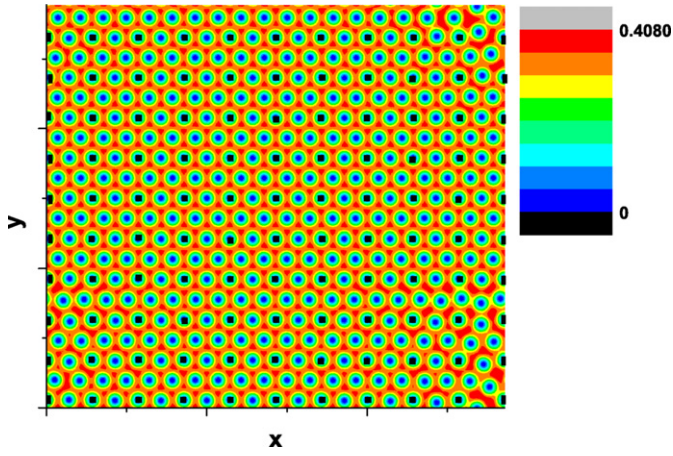


**Fig. 1.** Vortex distribution, pinning site locations (the black square), for the rectangular pinning array. The sizes for pinning centers are one (points), the magnetic field  $h = 0.4$ , and the temperature  $t' \simeq 0$ . The vortex lattice has hexagonal symmetry when electric field  $\epsilon = 0$ .

where the unit of current density is  $J_{GL} = cH_{c2}/(2\pi\xi\kappa^2)$  and the conductivity will be given in units of  $\sigma_0 = c^2\gamma/(4\pi\kappa^2)$ .

The continuum TDGL equation (Eq. (1)) is discretized using link variables

$$U_{n_1, n_2}^\mu = \exp\left(-i \int \mathbf{a}_{n_1, n_2} \cdot d\mathbf{r}^\mu\right), \quad (4)$$

$$\mathbf{a} = \left(-\frac{1}{2}hy, \frac{1}{2}hx - \epsilon\tau\right), \quad (5)$$

where  $\mu = x, y$  is the link direction. The electric field is applied in the  $y$ -direction and we use a symmetric gauge. The discretized TDGL equation is,

$$\begin{aligned} \frac{d}{d\tau} \psi_{n_1, n_2} = & \sum_{\mu=x, y} \frac{\sqrt{3}}{4} \frac{1}{a_\mu} \\ & \times [U_{n_1, n_2}^\mu \psi_{n_1+1, n_2} + (U_{n_1, n_2}^\mu)^* \psi_{n_1-1, n_2} - 2\psi_{n_1, n_2}] \\ & + \frac{\sqrt{3}}{2} \left[ \frac{(1-t)}{2} \psi_{n_1, n_2} - |\psi_{n_1, n_2}|^2 \psi_{n_1, n_2} \right], \end{aligned} \quad (6)$$

where  $a_\mu$  is the lattice spacing in the  $x$ - and  $y$ -direction. Periodic boundary conditions with magnetic translations [6] are used. The order parameters in the strong pinning centers are forced to be zero (always in normal state), while weak pinning are represented by step functions.

### 3. Simulation results

We consider three different pinning arrays. The pinning locations are on a square lattice in the first case and on a triangle in the second and the third cases. The pinning center sizes are one (point) in the first and second case and nine (points) in the third case. The magnetic field  $h = 0.4$  and the electric field are applied in the  $y$ -direction for all systems. Fig. 1 shows the configuration of a static vortex lattice with a rectangular pinning array (pinning size – one point); the vortex lattice still has a hexagonal symmetry, even though the pinning array is anisotropic. With the applied electric field, the interstitial vortices which parallel the pinning sites can flow along the  $x$ -direction, while the interstitial vortices between the pinning sites are obstructed by the pinned vortices, shown in Fig. 2. Fig. 3 shows a static vortex lattice with a triangular pinning array (pinning size – one point); the vortex lattice has a hexagonal structure. Like with rectangular pinning arrays, only the interstitial vortices can flow parallel the pinning sites, see Fig. 4.

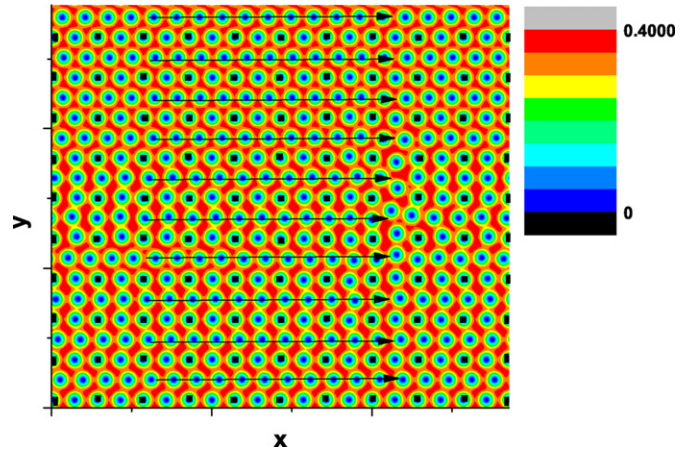


**Fig. 2.** Vortex distribution, pinning site locations (the black square), and vortex trajectories (the black lines, arrows are the direction) for the rectangular pinning array. The parameters are the same as in Fig. 1. The electric field is applied in the  $y$ -direction, the interstitial vortices which between the rows of pinning sites are moving in the  $x$ -direction, while the interstitial vortices in the rows of pinning sites cannot move.

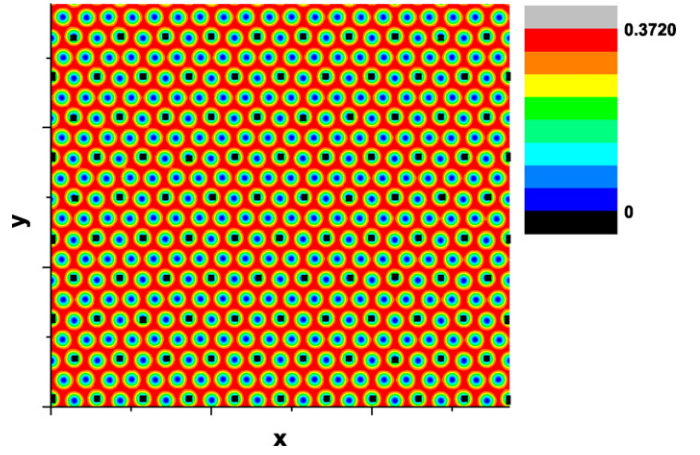


**Fig. 3.** Vortex distribution, pinning site locations (the black square) for the triangular pinning array. The sizes for pinning centers are one (points), the magnetic field  $h = 0.4$ , and the temperature  $t' \simeq 0$ . The vortex lattice has hexagonal symmetry when electric field  $\epsilon = 0$ .

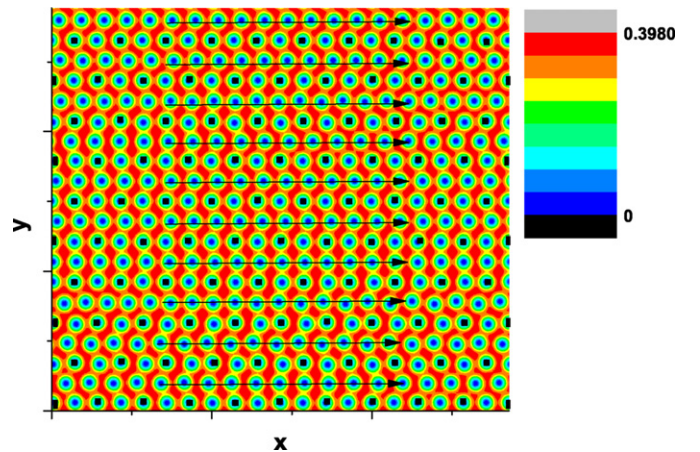


**Fig. 4.** Vortex distribution, pinning site locations (the black square), and vortex trajectories (the black lines, arrows are the direction) for the triangular pinning array. The parameters are the same as in Fig. 3. When the electric field is applied in the  $y$ -direction, the interstitial vortices which between the rows of pinning sites are moving in the  $x$ -direction, while the interstitial vortices in the rows of pinning sites cannot move.

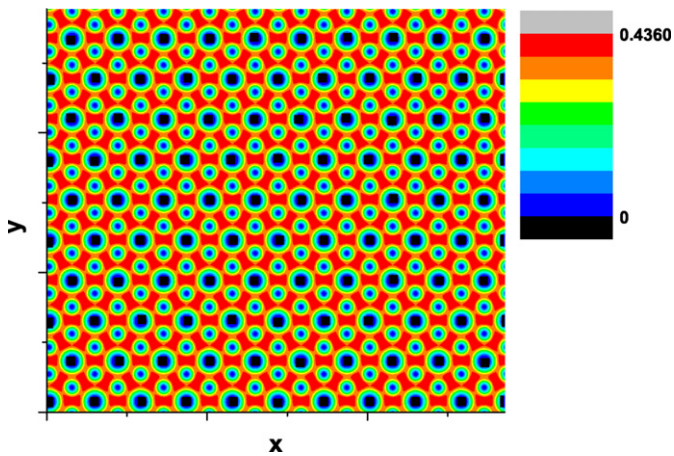


**Fig. 5.** Vortex distribution, pinning site locations (the black square). The sizes of pinning centers are one (points), the magnetic field  $h = 0.4$ , and the temperature  $t' \approx 0$ . The vortex lattice has hexagonal symmetry when electric field  $\epsilon = 0$ .

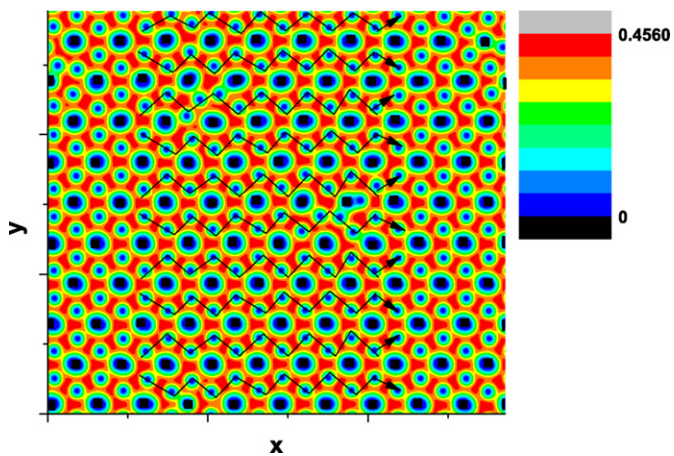


**Fig. 6.** Vortex distribution, pinning site locations (the black square), and vortex trajectories (the black lines, arrows are the direction) for the triangular pinning array. The parameters are the same as in Fig. 5. The electric field is applied in the  $y$ -direction, the interstitial vortices which between the rows of pinning sites are moving in the  $x$ -direction, while the interstitial vortices in the rows of pinning sites cannot move.

Fig. 5 shows the static vortex lattice with a triangular pinning array (pinning size – nine points); the configuration of the vortex lattice has a triangular symmetry, since the pinned vortices are larger than the interstitial vortices. Under electric field, unlike the previous cases, all the interstitial vortices are moving (Fig. 6). No vortices are effectively pinned. The shape of the pinned vortices is also influenced by the electric field and the interstitial vortices.

The  $\epsilon$ – $j$  characteristics with pinning effect are shown in Fig. 7. The number of pinning centers is equal to that of the vortices, which means that the system is at the first matching field. The resistivity is zero when the supercurrent density  $J < 1.58$ , since the vortices are caught by the pinning centers (the driving force being smaller than the pinning force), while when the supercur-

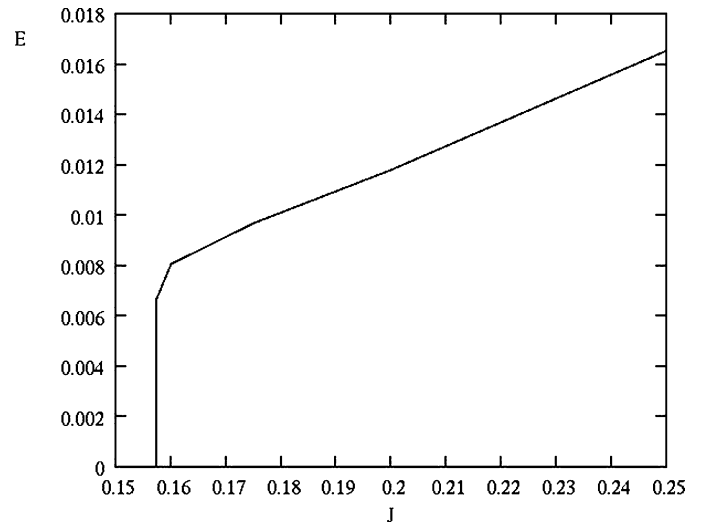


**Fig. 7.** The  $\epsilon$ – $j$  characteristic with pinning effect. The I–V curve approaches linear at large fields and exhibits pinning at a critical field.

rent density  $J > 1.58$ , the resistivity does not remain zero, since the vortices start moving (the driving force larger than the pinning force). When the supercurrent (density) equal to critical current (density), the driving force equal the pinning force.

#### 4. Conclusion

The configurations of vortex lattice above the first matching field for artificial pinning arrays are studied in this work. The vortex lattices are deformed by the pinning centers. For small pinning sizes, the vortex lattice has hexagonal symmetry whether in rectangular or triangular pinning arrays. For bigger pinning sizes (nine points), the symmetry for vortex lattices is no longer hexagonal and becomes triangular. The trajectories of interstitial vortices for small size pinning arrays like a line, only the interstitial vortices between the rows of pinning sites can move. The interstitial vortex trajectories for rectangular and triangular pinning arrays are similar. However, the trajectories for interstitial vortices with bigger size pinning array like a wave, the flowing interstitial vortices avoid the pinned vortices. For the vortices are caught by pinning array, the resistivity is zero when the supercurrent smaller than critical current, while the resistivity not remain zero when the supercurrent larger than the critical current.

#### References

- [1] M. Kemmler, et al., Phys. Rev. B 79 (2009) 184509.
- [2] J.I. Martin, et al., Phys. Rev. Lett. 79 (1997) 1929.
- [3] C. Reichhardt, C.J. Olson, F. Nori, Phys. Rev. Lett. 78 (1997) 2648; C. Reichhardt, C.J. Olson, Reichhardt, Phys. Rev. B 79 (2009) 134501.
- [4] T. Maniv, et al., Phys. Rev. B 80 (2009) 134512; B. Rosenstein, B. Shapiro, I. Shapiro, Phys. Rev. B 81 (2010) 064507.
- [5] A.A. Zhukov, et al., Physica C 404 (2004) 166; J.E. Villegas, et al., Phys. Rev. Lett. 97 (2006) 027002; Q.H. Chen, et al., Phys. Rev. B 78 (2008) 172507.
- [6] D.P. Li, et al., Phys. Rev. B 70 (2004) 214529; B. Rosenstein, D.P. Li, Rev. Modern Phys. 82 (2010) 109.